Ce:YIG/Silicon-on-Insulator waveguide optical isolator realized by adhesive bonding

S. Ghosh,[1,2,*] S. Keyvavinia,[1,2] W. Van Roy,[3] T. Mizumoto,[4] G. Roelkens,[1,2] and R. Baets[1,2]

[1]*Photonics Research Group, Department of Information Technology (INTEC), Ghent University, Sint-Pietersnieuwstraat 41, 9000 Gent, Belgium*
[2] *Center for Nano- and Biophotonics (NB-Photonics), Ghent University, Belgium*
[3]*Functional Nanosystems, Interuniversity Microelectronics Center (IMEC), Kapeldreef 75, B-3001 Leuven, Belgium*
[4]*Department of Electrical and Electronic Engineering, Tokyo Institute of Technology, 2-12-1 Ookayama, Meguro-ku, Tokyo 152-8552, Japan*
[*]*samir.ghosh@intec.ugent.be*

Abstract: A waveguide optical isolator realized by adhesive bonding of a garnet die, containing a Ce:YIG magneto-optic layer, on a silicon-on-insulator waveguide circuit is demonstrated. The die was bonded on top of an asymmetric Mach-Zehnder interferometer using a 100nm thick DVS-BCB adhesive bonding layer. A static magnetic field applied perpendicular to the light propagation direction results in a non-reciprocal phase shift for the fundamental quasi-TM mode in the hybrid waveguide geometry. A maximum optical isolation of 25 dB is obtained.

©2012 Optical Society of America

OCIS codes: (230.3240) Isolators; (160.3820) Magneto-optical materials.

References and links

1. K. E. Stubkjaer and M. B. Small, "Noise properties of semiconductor lasers due to optical feedback," IEEE J. Quantum Electron. **20**(5), 472–478 (1984).
2. O. Hirota and Y. Suematsu, "Noise properties of injection lasers due to reflected waves," IEEE J. Quantum Electron. **15**(3), 142–149 (1979).
3. R. W. Tkach and A. R. Chraplyvy, "Regimes of feedback effects in 1.5 µm distributed feedback lasers," J. Lightwave Technol. **4**(11), 1655–1661 (1986).
4. A. W. Fang, H. Park, O. Cohen, R. Jones, M. J. Paniccia, and J. E. Bowers, "Electrically pumped hybrid AlGaInAs-silicon evanescent laser," Opt. Express **14**(20), 9203–9210 (2006), http://www.opticsinfobase.org/abstract.cfm?URI=oe-14-20-9203.
5. H. Rong, R. Jones, A. Liu, O. Cohen, D. Hak, A. Fang, and M. Paniccia, "A continuous-wave Raman silicon laser," Nature **433**(7027), 725–728 (2005).
6. Y. Halioua, A. Bazin, P. Monnier, T. J. Karle, G. Roelkens, I. Sagnes, R. Raj, and F. Raineri, "Hybrid III-V semiconductor/silicon nanolaser," Opt. Express **19**(10), 9221–9231 (2011), http://www.opticsinfobase.org/abstract.cfm?URI=oe-19-10-9221.
7. H. Park, A. W. Fang, O. Cohen, R. Jones, M. J. Paniccia, and J. E. Bowers, "A hybrid AlGaInAs–silicon evanescent amplifier," IEEE Photon. Technol. Lett. **19**(4), 230–2232 (2007).
8. G. Roelkens, D. Van Thourhout, R. Baets, R. Nötzel, and M. Smit, "Laser emission and photodetection in an InP/InGaAsP layer integrated on and coupled to a Silicon-on-Insulator waveguide circuit," Opt. Express **14**(18), 8154–8159 (2006), http://www.opticsinfobase.org/abstract.cfm?URI=oe-14-18-8154.
9. H. Yokoi, T. Mizumoto, and Y. Shoji, "Optical nonreciprocal devices with a silicon guiding layer fabricated by wafer bonding," Appl. Opt. **42**(33), 6605–6612 (2003).
10. Y. Shoji, T. Mizumoto, H. Yokoi, I. W. Hsieh, and R. M. Osgood, Jr., "Magneto-optical isolator with silicon waveguides fabricated by direct bonding," Appl. Phys. Lett. **92**(7), 071117 (2008).
11. M. C. Tien, T. Mizumoto, P. Pintus, H. Kromer, and J. E. Bowers, "Silicon ring isolators with bonded nonreciprocal magneto-optic garnets," Opt. Express **19**(12), 11740–11745 (2011), http://www.opticsinfobase.org/abstract.cfm?URI=oe-19-12-11740.
12. S. Y. Sung, X. Qi, and B. J. H. Stadler, "Integrating yttrium iron garnet onto nongarnet substrates with faster deposition rates and high reliability," Appl. Phys. Lett. **87**(12), 121111 (2005).
13. T. R. Zaman, X. Guo, and R. J. Ram, "Semiconductor waveguide isolators," J. Lightwave Technol. **26**(2), 291–301 (2008).
14. A. K. Zvezdin and V. A. Kotov, *Modern Magneto-Optics and Magneto-Optic Materials* (Institute of Physics Publishing, 1997).

15. K. Postava, M. Vanwolleghem, D. Van Thourhout, R. Baets, S. Visnovsky, P. Beauvillain, and J. Pistora, "Modeling of a novel InP-based monolithically integrated magneto-optical waveguide isolator," J. Opt. Soc. Am. B **22**(1), 261–273 (2005).
16. F. Auracher and H. H. Witte, "A new design for an integrated optical isolator," Opt. Commun. **13**(4), 435–438 (1975).
17. T. Mizumoto, K. Oochi, T. Harada, and Y. Naito, "Measurement of optical nonreciprocal phase shift in a Bi-substituted $Gd_3Fe_5O_{12}$ film and application to waveguide-type optical circulator," J. Lightwave Technol. **4**(3), 347–352 (1986).
18. J. Fujita, M. Levy, R. M. Osgood, Jr., L. Wilkens, and H. Dötsch, "Waveguide optical isolator based on Mach-Zehnder interferometer," Appl. Phys. Lett. **76**(16), 2158–2160 (2000).
19. H. Dötsch, N. Bahlmann, O. Zhuromskyy, M. Hammer, L. Wilkens, R. Gerhardt, and P. Hertel, "Applications of magneto-optical waveguides in integrated optics: review," J. Opt. Soc. Am. B **22**(1), 240–253 (2005).
20. H. Yokoi, T. Mizumoto, N. Shinjo, N. Futakuchi, and Y. Nakano, "Demonstration of an optical isolator with a semiconductor guiding layer that was obtained by use of a nonreciprocal phase shift," Appl. Opt. **39**(33), 6158–6164 (2000).
21. D. Vermeulen, K. Van Acoleyen, S. Ghosh, S. Selvaraja, W. A. D. De Cort, N. A. Yebo, E. Hallynck, K. De Vos, P. P. P. Debackere, P. Dumon, W. Bogaerts, G. Roelkens, D. Van Thourhout and R. Baets, "Efficient tapering to the fundamental quasi-TM mode in asymmetrical waveguides," ECIO, United Kingdom, p.paper WeP16.
22. G. Roelkens, J. Brouckaert, D. Van Thourhout, R. Baets, R. Nötzel, and M. Smit, "Adhesive bonding of Inp/INGAASP dies to processed Silicon-On-Insulator wafers using DVS-Bis-Benzocyclobutene," J. Electrochem. Soc. **153**(12), G1015–G1019 (2006).

1. Introduction

Semiconductor lasers are widely used as light sources in optical communication systems. The stability and performance of the laser is very sensitive to back reflections from other components in the optical circuit [1–3]. In order to alleviate this issue, an optical isolator is highly desirable. In recent years many active optical components have been realized on the III-V/Silicon-on-Insulator platform [4–8]. Therefore, an optical isolator integrated on this platform is a stringent requirement for the stability of III-V/silicon lasers in future products. To realize an optical isolator a nonreciprocal medium is required. Waveguide-type optical isolators typically rely on the nonreciprocal phase shift (NRPS) a quasi-transverse magnetic mode experiences when interacting with such a medium, provided a static magnetic field perpendicular to the light propagation direction and to the dominant optical E-field is present. Nonreciprocal materials can be integrated on a silicon waveguide platform by means of bonding [9–11] or sputter deposition [12]. Sputter deposition is a wafer scale approach but the deposited film suffers from reduced Faraday rotation and large scattering loss compared to the bonding approach. Therefore, in this paper we adopt a die-to-wafer bonding technique based on adhesive bonding to integrate Ce:YIG, as the nonreciprocal medium, on top of a silicon waveguide circuit. The miniaturization of an optical isolator and its on-chip integration with other opto-electronic components on the silicon-on-insulator material platform has been pursued in recent years, resulting in on-chip optical isolators based on molecular bonding [10, 11]. In this work we use DVS-BCB as an adhesive polymer to bond Ce:YIG on silicon waveguide circuits, which is a more relaxed process in terms of surface roughness requirements and contamination control in order to achieve a good bonding quality. This approach paves the way to the heterogeneous integration of optical isolators with an integrated III-V/SOI semiconductor laser.

2. Isolator design

Commercially available pigtailed optical isolators consist of two polarizers with polarization axes offset 45° and a Faraday rotator usually using Yttrium Iron Garnet (YIG) as the nonreciprocal medium. An external longitudinal magnetic field is applied to the Faraday rotator, to obtain the nonreciprocal polarization rotation. Since high index contrast silicon waveguides are strongly birefringent, this bulk scheme cannot be efficiently implemented in a waveguide configuration [13], since a very stringent control over the waveguide cross-section is required. The device presented in this paper is based on the Voigt effect [14] in which the

static magnetic field is transverse to the light propagation direction. In the presence of an external magnetic field along the y-direction, the dielectric permittivity tensor takes the form given by Eq. (1)

$$\varepsilon = \begin{pmatrix} n^2 & 0 & j\varepsilon_{xz} \\ 0 & n^2 & 0 \\ -j\varepsilon_{xz} & 0 & n^2 \end{pmatrix} \tag{1}$$

where $j = \sqrt{-1}$ and n is the refractive index of the magnetic material. In this expression we neglect the second order magneto-optic contributions to the diagonal elements of the permittivity tensor. This permittivity tensor is non-symmetrical resulting in non-reciprocal behavior. This results in a difference in propagation constant between a forward and backward propagating mode, when light is propagating perpendicular to the applied magnetic field, e.g. along the z-direction. ε_{xz} is related to the Faraday rotation θ_F (degree/cm) as $\varepsilon_{xz} = n\lambda\theta_F / \pi$, with λ the wavelength. The nonreciprocal phase shift (NRPS) per unit length is calculated from the perturbation formula [15] as

$$NRPS = \beta_{Forward} - \beta_{Backward} = -j\omega\varepsilon_0 \frac{\iint \varepsilon_{xz}(x, y)E_x^0 E_z^0 dxdy}{\iint [E_x^0 H_y^0 - E_y^0 H_x^0]dxdy} \tag{2}$$

where E_i^0 and $H_i^0 (i = x, y, z)$ are the unperturbed field amplitudes of the optical mode, ω is the radial frequency and ε_0 is the free space permittivity. In a rectangular silicon waveguide the z-component of the electric field (E_z^0) of the fundamental quasi-TE mode is negligible compared to that of the quasi-TM fundamental mode. Hence appreciable NRPS is achieved for the quasi-TM fundamental mode only. Epitaxially grown Ce:YIG (Faraday rotation coefficient: −4500°/cm at 1.55µm, refractive index: 2.20) on a substituted Gadolinium Gallium Garnet (SGGG) substrate (refractive index: 1.94) is chosen as a magneto-optic material. The thickness of the Ce:YIG is about 260nm, grown on a 450µm thick SGGG substrate by sputtering. The layer stack after transfer to the SOI waveguide wafer is illustrated in Fig. 1(a). The resulting NRPS for the fundamental TM mode at 1.55µm for various DVS-BCB thicknesses and silicon waveguide layer thicknesses of the considered layer stack is shown in Fig. 1(b). The numerical integration is carried out considering a 2D slab structure. Since this is a 2D full–vectorial model, the NRPS obtained is approximately equal to that for a 900nm wide waveguide, as used in the experiments. The graph indicates that for a compact isolator, a thin DVS-BCB bonding layer is indispensible, but on the other hand the NRPS varies more slowly for larger DVS-BCB thicknesses such that the device will be more tolerant in this DVS-BCB thickness range. Since there will be a mismatch in the TM-mode field distribution at the interface between plain SOI and garnet-covered SOI, losses and parasitic reflections can be expected. The simulated transmission and reflection at such an interface is shown in Fig. 2. It is clear from this figure that the transmission loss and reflection reduce with increased DVS-BCB bonding layer thickness. As a consequence there is a tradeoff between device length, insertion loss and fabrication tolerance. As can be seen in the simulation results, a 220nm thick silicon waveguide layer thickness is quasi-optimal for all envisioned bonding layer thicknesses.
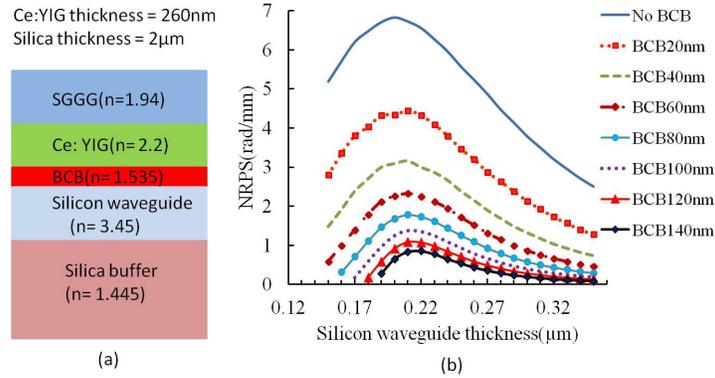
Fig. 1. (a) Slab waveguide stack and (b) simulation of the nonreciprocal phase shift as a function of silicon waveguide thickness and DVS-BCB bonding layer thickness.

The contour plot of the E_x^0 field in the actual waveguide cross-section is shown in Fig. 3(a). It is clear from the plot that the *x*-component of the electric field is discontinuous across the interfaces of the different layers. A vertical slot waveguide structure is formed between the silicon and Ce:YIG and the corresponding cross-sectional mode profile of E_x^0 is shown in Fig. 3(b). Mach-Zehnder Interferometer (MZI) type waveguide isolators have been investigated in several papers [9,10], [16–20]. Our MZI consists of two 1X2 multimode interference couplers (MMI), connected by two waveguides of unequal length. The MZI is partly covered by the Ce:YIG/SGGG die. Therefore, the design of the MMI covered by the nonreciprocal material is different from the one which is covered by DVS-BCB only. The length of the multimode section for the Ce:YIG covered MMI is 13.0µm whereas it is 11.0µm for the DVS-BCB covered MMI. The width of the multimode section and offset between output waveguides are designed as 4.0µm and 1.1µm respectively for both types of MMIs. A curved grating coupler is used to couple light between a single mode fiber and the quasi-TM fundamental mode of a 900nm wide silicon waveguide [21].
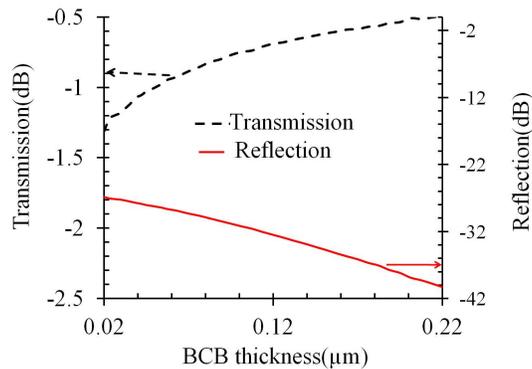

Fig. 2. Insertion loss and reflection at the interface between a plain SOI waveguide and a Ce: YIG on SOI waveguide as a function of DVS-BCB bonding layer thickness.
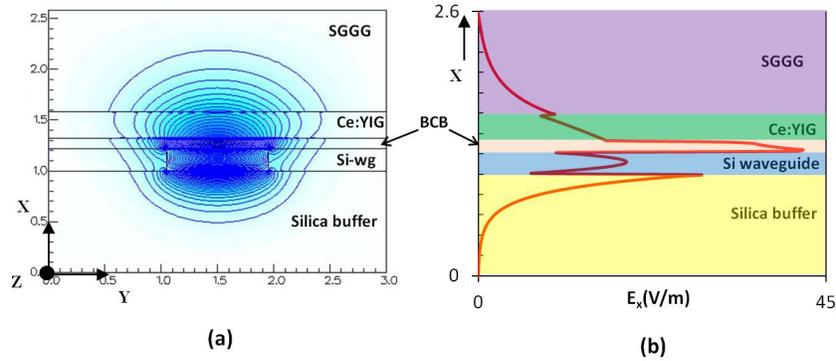
Fig. 3. (a) Contour plot of E_x^0 field of the quasi-TM polarized mode (b) field enhancement in the DVS-BCB bonding layer due to a vertical slot waveguide effect.

The length difference between the MZI arms is 80µm which results in a free spectral range of 7.6nm. This allows for a clear interpretation of the nonreciprocal phase shift. For a broadband device, equal arm lengths are required. The bend radius was limited to 60µm to avoid radiation loss in the Ce:YIG covered part of the silicon waveguide. The device layout is shown in Fig. 4. A unidirectional external magnetic field is applied transverse to the light propagation direction to achieve maximum isolation. The total length $L = L_1 + L_2$ of the waveguide interacting with the Ce:YIG (and where the magnetic field is oriented perpendicular to the propagation direction) is 920µm.
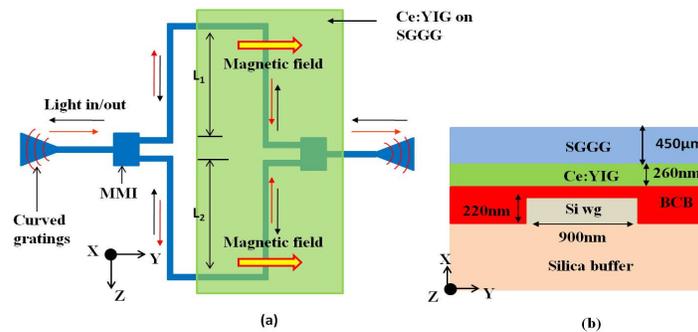

Fig. 4. Schematic of the proposed optical isolator consisting of a Mach-Zehnder interferometer covered by Ce:YIG; (a) top view and (b) cross- section view.
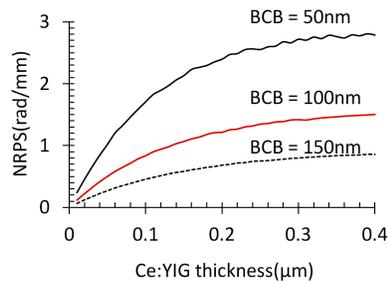

Fig. 5. Nonreciprocal phase shift as a function of Ce:YIG layer thickness for a 220nm thick silicon waveguide layer thickness and different DVS-BCB bonding layer thicknesses.

The nonreciprocal phase shift as a function of the Ce:YIG layer thickness, for a silicon waveguide layer thickness of 220nm, is shown in Fig. 5 illustrating that the 260nm Ce:YIG is sufficient to reach a high nonreciprocal phase shift.

3. Fabrication

The SOI waveguide circuits were fabricated in a CMOS pilot line using 193nm deep UV lithography. A 220nm thick silicon waveguide layer on a 2um buried oxide layer is used. The die-to-wafer bonding procedure is outlined in Fig. 6. Prior to bonding, the SOI dies are cleaned by a standard SC-1 cleaning procedure. Then adhesion promoter, AP3000 from Dow Chemicals, is spin coated on the SOI. Immediately afterwards mesithylene diluted DVS-BCB (1:3v/v) is spin coated at 5000 rpm for 50 seconds. Next, the SOI die is kept on a hot plate at 150°C for 3 minutes to evaporate the remaining mesithylene in the spin coated film. In parallel the garnet die is cleaned using acetone and isopropylalchohol (IPA). The garnet die (4mmx4mm) is aligned on top of the MZI, and in a final step the DVS-BCB is cured for about 3 hours following a standard DVS-BCB curing recipe. The details regarding the DVS-BCB bonding technique can be found in [22]. A photograph of the SOI chip with the Garnet die bonded on top is shown in Fig. 7 together with an SEM cross-section image of the bonded stack.
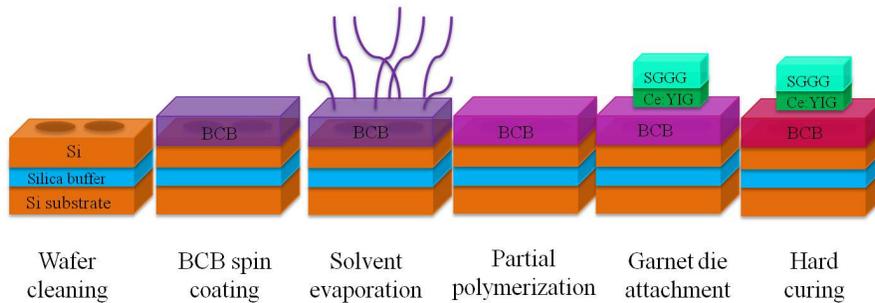

| Wafer cleaning | BCB spin coating | Solvent evaporation | Partial polymerization | Garnet die attachment | Hard curing |

Fig. 6. Schematic illustration of the bonding procedure.

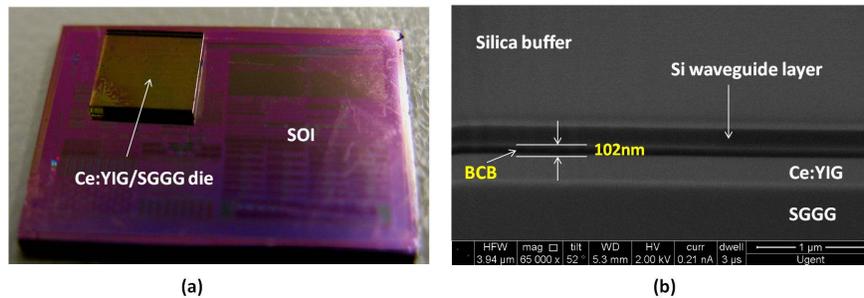(a)   (b)

Fig. 7. Photograph of the Ce:YIG/SGGG die bonded to an SOI waveguide circuit (a) and an SEM cross-section image of the bonded stack (b).

4. Experimental results

In the experiment small Neodymium-alloy (NdFeB) permanent magnets are used to provide the required transverse magnetic field. The dimensions of a single magnet are 3mm x 1mm x 1mm. A stack of three magnets is used to make sure that the magnetic field is almost parallel to the Ce: YIG plane. The layout of the experimental setup and magnet stack is shown in Fig. 8.
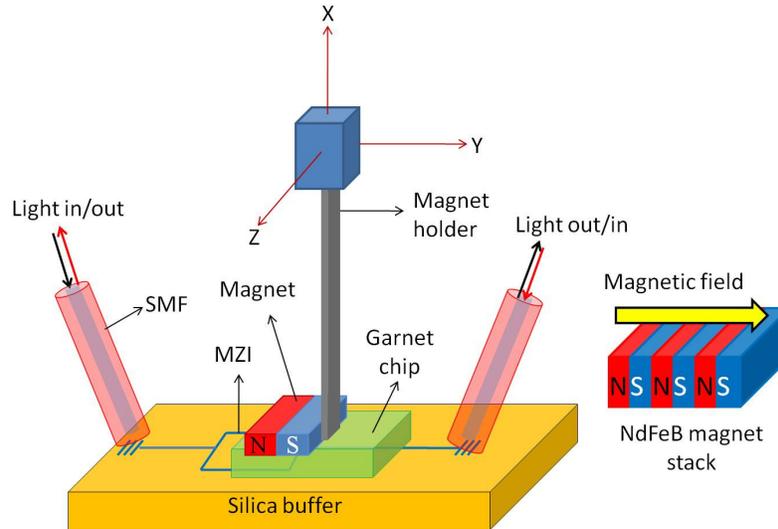
Fig. 8. Schematic diagram of measurement set up and magnet stack.

The magnetic field is estimated to be strong enough to saturate the Ce:YIG layer (the saturation field strength of the Ce:YIG is about 50 Oe). TM light is injected and collected by curved TM grating couplers. Transmission spectra were recorded both for the forward and backward propagation direction to characterize the MZI as an optical isolator. The corresponding spectra are shown in Fig. 9.
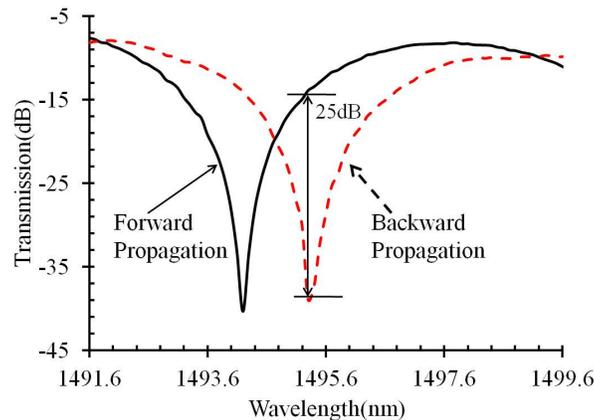

Fig. 9. Normalized MZI transmission spectra for forward and backward propagation.

Experimentally an optical isolation of 25 dB is achieved. A spectral shift of 1.1nm is measured between the forward and backward propagation under the influence of an external magnetic field. This spectral shift corresponds to an accumulated nonreciprocal phase shift ($\beta_{Forward}$ - $\beta_{Backward}$)*L of 52°. With L = 920um, this corresponds to a difference in propagation constant between the forward and backward direction of 0.987 rad/mm. Projecting the measured NRPS on the simulation results, this corresponds to a DVS-BCB thickness in the range of 100nm-120nm, which is in accordance with the targeted value.
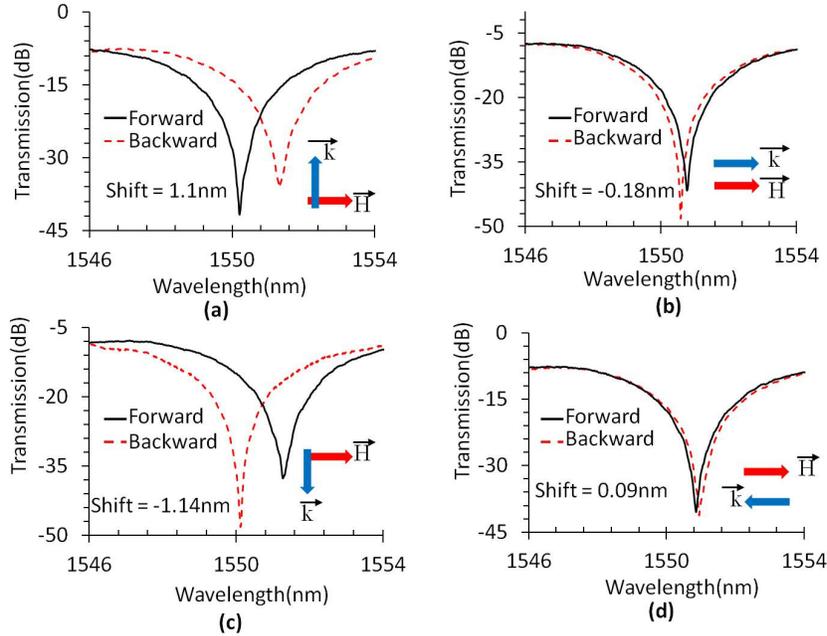
Fig. 10. Normalized transmission spectra of the MZI for different angular orientations of magnetic field with respect to the light propagation direction: (a) 90°, (b) 0°, (c) 270°, (d) 180°.

The influence of the applied magnetic field (H) orientation with respect to the propagation direction (k) was also assessed. The result is presented in Fig. 10. In the experimental setup the magnet is rotated from 0° to 360° around the X-axis (see Fig. 8). The rotation of the magnet was carried out away from the Ce:YIG (i.e. by lifting the magnet). For each magnet orientation forward and backward transmission was recorded. The nonreciprocal wavelength shift is taken to be negative when the transmission spectrum for forward propagation is shifted towards longer wavelengths compared to the backward propagation. The wavelength shifts (or NRPS) both for 0° and 180° orientations are very small as compared to 90° and 270° orientations, which is a signature of the Voigt effect. The variation of the nonreciprocal wavelength shift with respect to $(h^2 + l^2)^{-3/2}$ is presented in Fig. 11(a), where h is the distance between the garnet die and the magnet and 2l (3mm) is the pole to pole distance of the magnet stack. The reason behind choosing $(h^2 + l^2)^{-3/2}$ as a parameter is that the magnetic field at broadside-on position of a bar magnet varies as $(h^2 + l^2)^{-3/2}$ .The sequence of the measurements is illustrated in the Fig. 11(a). In part 1 of the curve the magnet is oriented perpendicular to the Ce:YIG covered Mach-Zehnder arms (say N-S orientation) and the forward and backward transmission is recorded for each increment of the distance between the magnet and the Ce:YIG. At the remanent point the magnet orientation was rotated 180 degrees to S-N for part 2 of the curve, where the magnet stack approaches the garnet die. The nonreciprocal wavelength shift at the remanent condition is about 0.6nm. In part 3 of the curve, the distance between the magnet with S-N orientation and the Ce:YIG die is increased again. Finally, in part 4 of the curve the magnet again switches to N-S and the nonreciprocal wavelength shifts were recorded for each decrement of the distance. The parameter $(h^2 + l^2)^{-3/2}$ is taken to be positive & negative for N-S & S-N orientations respectively. The stability of the residual magnetization over time of the Ce:YIG die is also tested in terms of nonreciprocal wavelength shift without applying any external magnetic field for three months. The nonreciprocal wavelength shift for the residual magnetization remained 0.6nm after three months. This suggests that the residual magnetization of Ce:YIG film is permanent

at-least for three months. The magnetization of the Ce:YIG film of thickness 260nm is also measured by an alternating gradient force magnetometer (AGFM).The magnetization curve of Ce:YIG film is shown on Fig. 11(b). Clearly there is a very good similarity between these two curves.
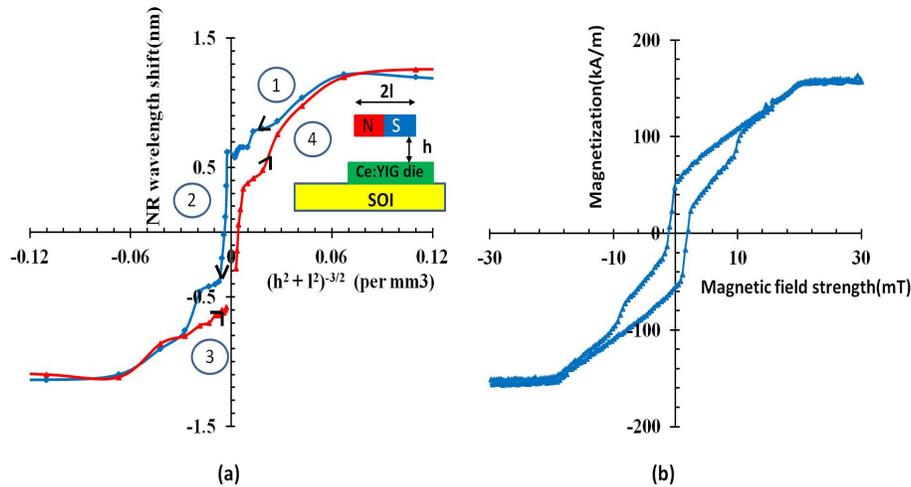

Fig. 11. (a) Nonreciprocal wavelength shift as a function of $(h^2 + l^2)^{-3/2}$, where h is the distance between the magnet and the Ce:YIG layer and 2l is the distance between the two poles of the magnet stack. Negative values for $(h^2 + l^2)^{-3/2}$ indicate that the magnet was rotated 180 degrees, (b) magnetization curve of the Ce:YIG layer after subtracting the contribution from the paramagnetic SGGG substrate.

As can be seen on the transmission spectra, the insertion loss of the Mach-Zehnder structure is 8-9dB at the constructive interference point. Since the obtained nonreciprocal phase shift is less than 180 degrees, the insertion loss at the maximum optical isolation point is around 14dB. This implies that for a high isolation, broadband MZI isolator, a 3.46 times (52 degrees non-reciprocal phase shift versus the requires 180 degree phase shift) longer Ce:YIG/SOI nonreciprocal waveguide section is required. The relatively high insertion losses of the device are due to a combination of mode mismatch losses at the interface between the plain SOI and the SOI covered with the diced Ce:YIG die (see Fig. 4) and propagation losses in the Ce:YIG/SOI waveguide structure. The propagation loss of the Ce:YIG/SOI waveguide structure was assessed experimentally by comparing transmission spectra of a Ce:YIG covered SOI waveguide (using a 100nm DVS-BCB bonding layer) and a plain SOI waveguide. The excess loss of the SOI waveguide structure covered by a 2mm long garnet die is 4dB compared to plain SOI waveguide. Taking into account the theoretical transition losses from Fig. 2 (2 times 0.8dB) this results in a Ce:YIG/SOI waveguide propagation loss of 12dB/cm (4dB-2x0.8dB)/2mm) in excess of the 2.5 dB/cm propagation loss of a standard SOI waveguide, resulting in an overall propagation loss of 14.5dB/cm. The cause of this large excess waveguide loss could not be unambiguously identified, but can be attributed to scattering and propagation losses in the Ce:YIG combined with the larger sensitivity of the Ce:YIG/SOI quasi-TM waveguide mode to Ce:YIG surface roughness, due to the slot waveguide field enhancement effect in the bonding layer. Given the 4mm x 4mm Ce:YIG/SGGG die size in the experimental realization, this results in approximately 4.5mm of Si wire waveguide covered with Ce:YIG. Taking these propagation losses into account, together with the interface losses, this amounts to a total insertion loss of 2x0.8 dB + 14.5 dB/cm*0.45 cm or 8.1 dB, which is close to the measured insertion loss. It also means that if the Ce:YIG/SGGG die size was reduced, such as to only cover the arms of the Mach-Zehnder interferometer, while the Ce:YIG/SOI waveguide length inside the MZI interferometer was

increased by a factor of 3.46 (to obtain 180 degree nonreciprocal phase shift), the insertion loss could be reduced to 2x0.8 dB + 14.5 dB/cm*3.46*0.46 mm or 3.9 dB.

5. Conclusions

In this paper we have demonstrated an optical isolator integrated on the silicon-on-insulator platform by adhesively bonding a Ce:YIG/SGGG die to a silicon waveguide circuit. The nonreciprocal phase shift (NRPS) or nonreciprocal wavelength shift has been studied both for transverse and longitudinal magnetic fields with respect to light propagation direction. The hysteresis behavior of the Ce:YIG film is also studied. While optical isolation and insertion loss of the device still can be optimized this approach opens a promising path towards the heterogeneous integration of an optical isolator with semiconductor lasers on the SOI platform.